Fall 7-17-2018

Thermo-Mechanical Response of Self-Assembled Nanoparticle Membranes

Yifan Wang

Henry Chan

Badri Narayanan

Sean P. McBride
Marshall University, mcbrides@marshall.edu

Subramanian K.R.S. Sankaranarayanan

See next page for additional authors

Recommended Citation

Wang, Y., Chan, H., Narayanan, B., McBride, S. P., Sankaranarayanan, S. K. R. S., Lin, X. M., Jaeger, H. M. (2017). Thermomechanical Response of Self-Assembled Nanoparticle Membranes. ACS Nano 11(8), 8026-8033. doi: 10.1021/acsnano.7b02676

Authors
Yifan Wang, Henry Chan, Badri Narayanan, Sean P. McBride, Subramanian K.R.S. Sankaranarayanan, Xiao-Min Lin, and Heinrich M. Jaeger

Thermo-Mechanical Response of Self-Assembled Nanoparticle Membranes

Yifan Wang[1,2], Henry Chan[3], Badri Narayanan[3], Sean P. McBride[4], Subramanian K.R.S. Sankaranarayanan[3], Xiao-Min Lin[3] and Heinrich M. Jaeger[1,2]

[1]Department of Physics, University of Chicago, 5720 S. Ellis Avenue, Chicago, Illinois 60637, United States
[2]James Franck Institute, University of Chicago, 929 E. 57th Street, Chicago, Illinois 60637 United States
[3]Center for Nanoscale Materials, Argonne National Laboratory, 9700 South Cass Avenue, Argonne, Illinois 60439, United States
[4]Department of Physics, Marshall University, One John Marshall Drive, Huntington, West Virginia 25755, United States

Ultrathin membranes composed of metallic or semiconducting nanoparticles capped with short ligand molecules are hybrid materials that have attracted considerable research interest.[1-12] In contrast to two-dimensional (2D) membranes such as graphene and transition metal dichalcogenides monolayers, nanoparticle membranes can be engineered to achieve widely tunable mechanical, electronic or optical properties through different combinations of inorganic cores and organic ligands. In terms of mechanical properties, these membranes can form large area (tens of microns in diameter) freestanding structures with high Young's moduli (~GPa) and fracture strength.[1,13-15] Molecular dynamics (MD) simulations have indicated how this mechanical robustness can arise from van der Waals interactions between interdigitated ligands and how it is linked to the arrangement of these ligands in the space between neighboring particles.[16-21] These simulations furthermore make a number of specific predictions regarding the thermo-mechanical behavior of nanoparticle membranes. To date, however, there have been no systematic experimental realization and tests of these predictions.

Here, we report the first experiments that investigate the thermo-mechanical response by directly measuring their Young's moduli at elevated temperatures. Qualitatively consistent with predictions from molecular simulations, we observe a decrease of Young's modulus as temperature increases. However, this change is non-reversibly hysteretic during the first annealing cycle, a phenomenon that is not predicted by previous numerical work.[17,21] Using coarse-grained molecular dynamics (CGMD) simulations, we attribute this behavior to a spatial reorganization of the ligands. This reorganization proceeds from an initially asymmetric ligand arrangement around the nanoparticle, as a result of the membrane self-

assembly process at a water-air interface,[22] to a more symmetric spatial distribution. We then demonstrate that this hysteresis can be largely mitigated in two ways: by controlling the initial ligand packing density or by crosslinking the ligands with electron beam exposure. Furthermore, for a given ligand distribution, the membrane's mechanical stiffness was found to depend significantly on humidity. We associate this with partial screening of ligand-ligand interactions by a small amount of water molecules entering the interstices between particles. Overall, our results not only provide a more in-depth understanding on how the molecular-scale ligand arrangement between nanoparticles affects the macroscopic mechanical behavior of a membrane as a whole, but they also demonstrate new possibilities to control this behavior by targeting the ligand-mediated particle interactions directly, without changing the ligand chemistry.

In our experiments, Au nanoparticles with ~5.2nm diameter were synthesized with a digestive ripening method,[23] and coated with ~1.7nm long dodecanethiol ligands. Monolayers of Au nanoparticles were assembled at a water-air interface and draped over a carbon coated Transmission electron microscopy (TEM) grid with prefabricated 2μm diameter circular holes. The nanoparticle monolayers were strong enough to form freestanding membranes over these holes. Scanning electron microscope (SEM, **Figure 1a**) and TEM, (**Figures 1b&c**) were used to image the locally ordered particle arrangements before and after thermal annealing. Atomic force microscopy (AFM, **Figure 1d**) topography images showed the monolayers recessed into the holes by 20-30nm, giving rise to slightly pre-stressed, smooth membranes with height fluctuations of <5nm.

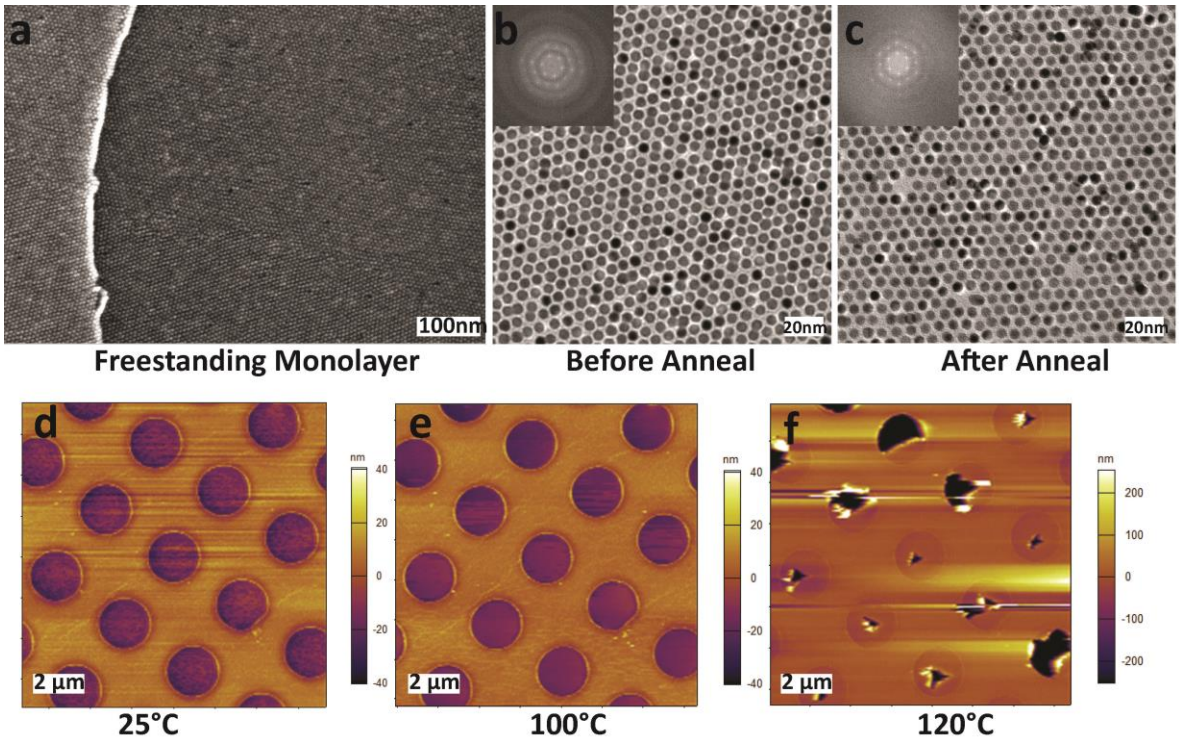

Figure 1 (a), SEM image of freestanding nanoparticle monolayer across a 2µm diameter hole on carbon TEM grid. **(b,c)**, TEM image of freestanding nanoparticle monolayer before and after annealing at 80°C, the inset shows FFT of these nanoparticle lattices, the change of lattice constant is not detectable within resolution. **(d-f),** AFM scanning images of nanoparticle monolayers at different temperatures. The monolayer stays intact till 100°C, but starts to rip and fracture at 120°C.

To assess the thermal stability the membrane, samples were loaded into an enclosed sample cell in a nitrogen environment, and the temperature was systematically varied from 10°C to 120°C. After very gentle indentations (~5nN) at each temperature, AFM tapping mode images were recorded to check the integrity of the membrane (**Figures 1d-f**). We found that the freestanding membranes possess considerable mechanical stability up to 100°C. Only above 100°C did the membranes become fragile and easy to break upon indentation. Most membranes ripped and fractured after 5nN AFM indentation at 120°C (**Figure 1f**). This is in contrast to previous MD simulation results[16,17] that predicted surface ligand melting at ~20°C and Young's modulus vanishing at ~50-60°C in 3D gold-dodecanethiol superlattices.

To measure the mechanical properties of the membranes more quantitatively, we used AFM to indent the centers of the membranes at each temperature. Typical data are shown

in **Figure 2a**, indicating linear behavior at small indentation and nonlinear behavior with higher stiffness under large indentation. To extract the membranes' intrinsic mechanical properties from such force curves, we used a previously developed model of a linear elastic disk clamped along the circumference that is subjected to center loading. The force response F and indentation depth δ can be related by:[1,13]

$$F = \sigma^{2D}\pi\delta + E^{2D}(q^3R)(\frac{\delta}{R})^3 \quad (1)$$

Here σ^{2D} is the pre-stress in the membrane from both the fabrication process and the clamping along the perimeter; $R = 1\mu\text{m}$ is the radius of the membrane; q is a constant depending on the Poisson ratio ν (q=1.02 in our case where $\nu = 0.34$);[24] E^{2D} is the 2D Young's modulus of the membrane, related to the 3D Young's modulus E by $E^{2D} = E \cdot t$ where $t = 7\text{nm}$ is the physical membrane thickness including the diameter of the nanoparticle core and the thickness of the ligand shell.[14] Using this model, we fit the experimental force-indentation curves to **Equation 1** and obtain the fitting parameters σ^{2D} and E. At room temperature (25°C) in dry nitrogen environment, we found $\sigma^{2D} = 0.44 \pm 0.04\text{N/m}$ and $E = 19 \pm 3\text{GPa}$. Given the fact that there are no covalent bonds between the ligands from neighboring nanoparticles, the high Young's modulus is quite remarkable.[1,13] From this fit we also obtain the pre-strain $\varepsilon_0 = \frac{\sigma^{2D}}{Et} = 0.3\%$, a value well below the failure strain (~1.6%) measured previously.[14]

Young's moduli were analyzed at different temperatures from 5°C to 90°C (**Figures 2a&b**). At each temperature, ten membranes were measured and averaged. The membrane Young's modulus is seen to decrease from ~21GPa at 5°C to ~8GPa at 90°C during heating process. This almost 60% decrease clearly indicates the importance of the ligand interactions[16-21], since the van der Waals interaction between gold cores does not change significantly within this temperature range. Upon cooling, the monolayers regain their stiffness only partially, back to ~12GPa at 10°C. This large hysteresis during the heating-cooling cycle is in contrast with previous simulation results,[17,21] which predict that any weakening due to temperature-induced ligand disorder should be completely reversible. However, this hysteresis is not found in the second and subsequent heating-cooling cycle (**Figure 2c&d**), where the modulus-temperature dependence is also less than the first cycle.

These results indicate that the hysteretic thermo-mechanical response during the first annealing cycle is related to an irreversible change of the ligand configuration.

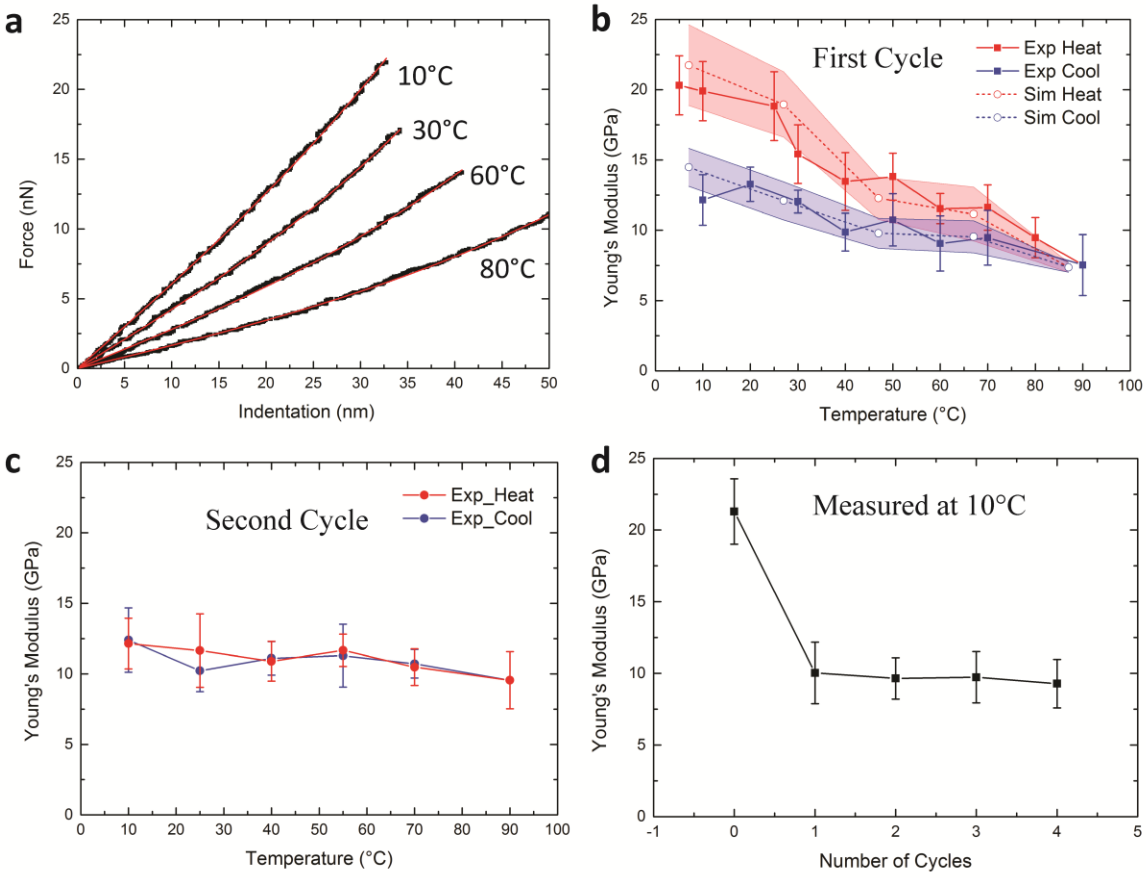

Figure 2 (a) Force-indentation curves of freestanding monolayers at different temperatures from 10°C to 80°C measured in dry nitrogen environment, black curves are measured data and red lines are fittings from Equation 1. (**b)** Change of Young's moduli after the first heating (red) and cooling (blue) cycle, with error bar shows the standard deviation over ~10 samples. The shaded region centered on the dash lines shows MD simulations results on a ~0.28 nm^2/ligand coverage sample with errors, which are scaled by a constant factor of 12.2 to overlay with the experimental curves. (**c**) The monolayer Young's moduli for the second heating-cooling cycle. (**d)** Membrane Young's moduli measured at 10°C after different number of heating-cooling cycles.

To investigate this behavior in more detail and link the experimental results with temperature-induced changes at the molecular scale, we performed CGMD simulations (see methods for details). A periodic simulation box comprised of a 16-nanoparticle supercell was used to model the membrane. The ligand surface coverage was ~ 0.28 nm^2/ligand, which corresponds to a membrane formed from ligand-deficient nanoparticle

samples subjected to extensive washing after nanoparticle synthesis as discussed previously.[22] The membrane was subjected to uniaxial tensile tests under a heating-cooling cycle. The potential energy plot in **Figure 3a** shows the heating-induced change in membrane configurations to energetically (~3 kcal/mol/ligand) more stable ones. Young's moduli obtained from the slope of stress-strain curves (**Figure 3b**) at different temperatures, averaged over 8 membrane configurations and scaled by a constant factor of 12.2, reproduce the exact degree of change and hysteretic behavior in thermo-mechanical response observed in experiment (**Figure 2b**). Note that our simulations as well as previously reported atomistic simulations[17,21] under predict the Young's modulus of the membranes compared to experiments. In our case, we used the default parameters for Martini model as listed in method section. We believe that the >10 times difference between the experimental and our as well prior simulation results might stem from the use of force field parameters that were not explicitly fitted to reproduce the elastic properties of nanoparticle membranes. The experimental membranes are stiffer compared to those in the simulations. Indeed, when the core-ligand and ligand-ligand interactions in the potential energy function are made stronger in the simulations, we find that the membranes tend to be stiffer. Scaling the ligand-ligand interactions by a scaling factor of 6 can lead to a 3-fold increase in the predicted Young's modulus values with a small 0.6% change in inter-particle separations.

Analysis of the simulation trajectories reveals collective microscopic rearrangement of nanoparticle ligands as the cause of the hysteretic behavior. As shown in **Figure 3c**, the distribution of ligands around a single nanoparticle in the as-prepared membranes is asymmetric due to the self-assembly process of the monolayers at an air-water interface,[22] but the low coverage of ligands coupled with ligand mobility at high temperatures ~ 87º C allows ligands to reorganize on nanoparticle surface to achieve a near-uniform symmetric distribution. This ligand rearrangement results in a corresponding change in the number of interdigitating ligands and/or their conformation. We quantify ligand conformational changes using an order parameter defined by the angle between the end-to-end vector of a ligand molecule (**Figure 3d**). The density maps in **Figure 3e** show the relative change in number of interdigitated ligands in the membrane during heating at 87º C and upon cooling

to 7º C. During the heating phase, we notice only a small change in the ligand conformation as seen by the small shift in the probable angle of θ_p ~89°-90°. This "probable angle" represents the angle corresponding to the peak in the Gaussian distribution of the angle between interdigitating ligands computed from MD trajectories. The distribution of this angle shifts from an initial probable angle of θ_p ~89°-90° to θ_p ~85-88° during cooling. The subtle change in θ_p leads to better contacts between interdigitating ligands, which might translate to more robust membranes that show a reversible mechanical behavior but lowered overall Young's moduli (**Figures 2c&d**). The transformation in the number of interdigitated ligands of an as-prepared membrane during the heating-cooling cycle is illustrated in **Figure 3e**. Upon heating to 87° C, the density maps suggest a decrease in the number of interdigitating ligands occurs as a result of ligand rearrangement due to reduced barriers. Although the number of interdigitating ligands increases again upon cooling to 7° C, the final value is about 2% lower compared to the initial configuration at 7° C. The observed hysteresis in Young's modulus with temperature is thus partly due to this subtle change in the number of interdigitated ligands during the annealing process.

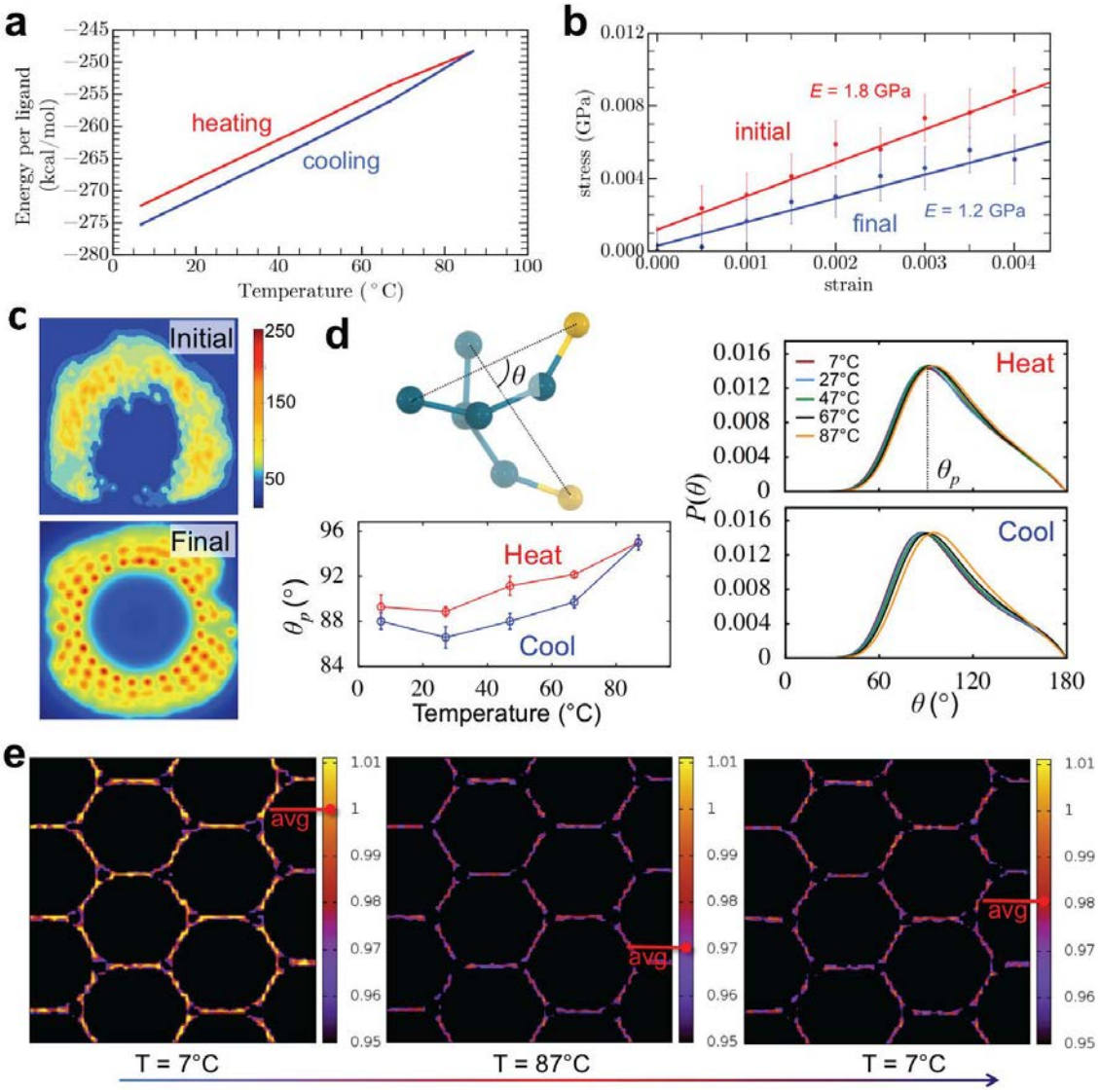

Figure 3. Structural evolution of freestanding monolayers during an annealing (heat-cool) cycle as obtained from CGMD simulations. **(a).** Change in potential energy as a function of temperature, and **(b)** significant difference in stress-strain behavior (at strain rate of 2.5×10^{-4}/ns, ligand coverage ~0.28 nm^2/ligand) between the initial and final samples at 7°C. **(c).** Distribution of ligands around a typical nanoparticle before (initial) and after (finial) the heat-cool cycle. **(d).** Angular distribution between the end-to-end vectors of interdigitating ligands on neighboring gold nanoparticles (as depicted in the schematic) at different temperatures. In the schematic image, the ligand beads that bind to a nanoparticle are shown in yellow, while others are depicted in blue. **(e).** Time-averaged number density maps showing the changes in interdigitated ligands during an annealing cycle. We calculate the number of interdigitating ligands based on a distance criterion *i.e.* by summing and averaging over all the ligands belonging to neighboring gold nanoparticles and located within a cut-off of 7 Angstrom (chosen from the first nearest neighbor distance from the radial distribution function calculated for ligands from different particles). The number of interdigitated ligands decreases during a heating

phase from 7° C to 87° C but partially recovers during the subsequent cooling back to 7° C. The color scale is normalized with respect to the initial membrane configuration at 7° C and the relative change in color corresponds to fractional change in number density.

Having established this molecular origin of the hysteresis during first thermal cycle, an interesting question arises as to how this hysteresis can be controlled. One approach is to reduce the initial ligand packing asymmetry. This can be achieved by adding excess dodecanethiol ligands to the nanoparticle solution, which suppresses the asymmetry by maximizing the overall ligand packing density.[22] **Figure 4a** confirms that the hysteresis is much reduced in fully ligated membranes. At the same time, the increase in ligand density increases the inter-particle spacing.[22] As a consequence, the degree of interdigitation between ligands from neighboring particles is reduced. This explains the reduction in Young's modulus (~40%) compared to the data in Fig. 2b.

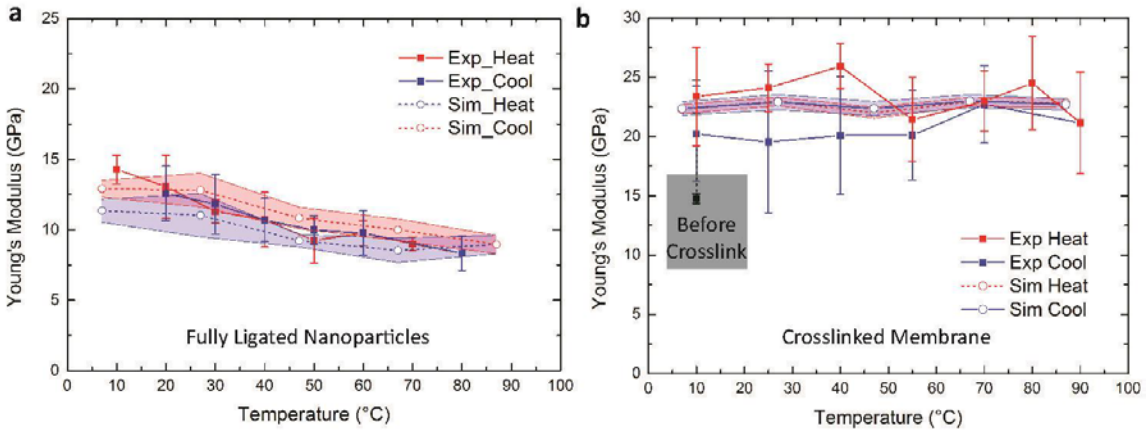

Figure 4. Controlling the hysteretic thermo-mechanical behavior. **(a)** The Young's moduli and temperature dependence of a fully ligated nanoparticle monolayer. **(b)** Monolayer Young's moduli before and after crosslinked with electron beam. Solid points and lines are experimental data. The dash lines with shaded region show the MD simulations results with errors. The simulation data are multiplied by the same constant scaling factor used in Figs. 2 and 3 to overlay the experimental trend. Cross-linking in the simulations was achieved by defining a rigid bond between beads of ligands that belong to different gold nanoparticles and are located within a cut-off of 7 Angstrom (chosen from the first nearest neighbor distance from the radial distribution function calculated for ligands from different particles).

A second approach to control the hysteresis is to constrain ligand rearrangements by crosslinking. Studies on self-assembled monolayers (SAMS) have shown that electron

beams can cause C-H, C-C, and C-S bond cleavage which leads to new C=C bond formation and crosslinks the monolayer.[25] We exposed the membranes with a sufficiently large electron beam dose[24] (~25mC/cm^2 at 10keV) in a SEM. Young's moduli of these membranes show an increase by ~50% after exposure and stay almost unchanged from 10°C to 90°C, with very little hysteresis (**Figure 4b**). The same trends are observed in the simulations.

The evidence from the data discussed so far indicates that ligand-ligand interactions control the mechanical behavior of the membranes, and in particular their tensile stiffness as characterized by Young's modulus. We can test this in yet another way, namely by directly modifying the strength of this ligand-ligand interaction. Given that the van der Waals forces between ligands are related to electrostatic dipolar interactions, the introduction of water molecules adsorbed on the surfaces and cavities in the membrane with high dielectric constant,[26,27] is expected to significantly screen the interactions between ligands, and thus reduce the mechanical stiffness. To verify this, we measured the Young's moduli of freestanding monolayers in air with ~40% humidity instead of dry nitrogen (**Figure 5a**). The results show a significant drop in modulus below room temperature (~25°C). While the membrane exhibits the same type of hysteresis during the cycling to high temperature as the data in **Figure 2b**, one distinct difference is that the modulus drops significantly upon cooling below room temperature. This can be attributed to condensation of water vapor on the membrane. To prove this, the moduli were measured while switching from dry nitrogen to "wet" nitrogen, with ~90% humidity, produced by bubbling dry nitrogen through a container filled with water. The results (**Figure 5b**) show that the monolayer modulus can be controllably and repeatedly weakened by wet nitrogen, while it recovers when switched to dry nitrogen. The reason the data in this figure do not recover the initial value is the water molecules trapped in the membranes once "wet" cannot evaporate fully during the 30min cycle period. Due to this reason, our nanoparticle monolayers which was originally very "wet" after assembled at water-air interface, were left over 24 hours for the water to completely evaporate, before high Young's moduli were measured in all previously described experiments.

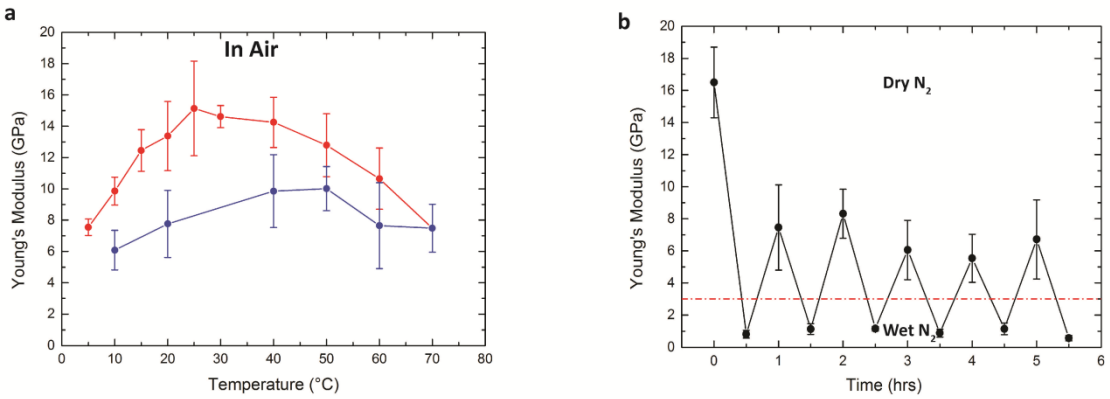

Figure 5. (a) Monolayer Young's moduli and temperature dependence measured in ~40% humidity air. The red and blue data plot represents the heating and cooling process, respectively. (**b)** Monolayer Young's moduli measured at 25°C in switching dry and wet nitrogen environment. The dashed red line at 3GPa is an artificial guideline to separate the measurements in dry and wet nitrogen.

In summary, our results demonstrate that the thermo-mechanical behavior of freestanding nanoparticle membranes is intricately linked to the ligand distribution around the nanoparticle and how effectively the ligands from neighboring particles can interact. One consequence is a pronounced hysteresis in the membrane's Young's modulus during thermal cycling. Using CGMD simulations we traced the origin of this hysteresis to irreversible changes in the molecular scale ligand conformation and reorganization. We then demonstrated that the hysteresis can be controlled, and removed, by suppressing the ability of the ligands to rearrange with temperature, either by maximizing the ligand packing density or by crosslinking them through e-beam irradiation. For example, hysteresis is observed at partial ligand surface coverage and not seen at full coverage. Finally, we showed that screening the ligand interactions by introducing water vapor provides a direct, and reversible, means of modulating the mechanical stiffness. The findings indicate a remarkable robustness of these ultrathin membranes, retaining Young's moduli in the GPa range up to temperatures approaching 100^0C, significantly higher temperatures than expected based on prior simulation results.

Methods. The Au nanoparticles with diameters of (5.2 ± 0.3nm) capped with dodecanethiol ligands were synthesized using a digestive ripening method. The nanoparticles were washed extensively by ethanol for 3 times and re-suspended in toluene.

A volume concentration of 10^{-4} dodecanethiol was back added to the nanoparticle solution, previous results have shown that this ligand concentration is not sufficient to cover the entire nanoparticle surface. To fully cover the nanoparticle surfaces, a higher volume concentration of 5×10^{-4} was added to the washed nanoparticle solution for comparison. In order to make freestanding nanoparticle monolayers, a carbon coated TEM grid (Quantifoil 657-200-CU from Ted Pella) with 2μm holes was placed on a PTFE substrate, and a 100μL distilled water droplet was deposited on the substrate covering the TEM grid. Then 10μL of nanoparticle solution was added to the edge of the water droplet. The nanoparticles immediately climbed to the air-water interface and formed a raft, which further grew and covered the entire surface. The water droplet with nanoparticle monolayer was left to dry for 5-6 hours and the monolayer eventually draped itself onto the carbon grid, forming freestanding monolayers spanning across the holes.

A Carl Zeiss Merlin SEM was used to image the freestanding nanoparticle monolayers down to individual nanoparticle resolution and crystalline structures with ~μm size domains were found (**Figure 1a**). The same SEM was also used to expose electron beam onto freestanding monolayers and crosslink the ligands between nanoparticles in later experiments. A Tecnai F30 TEM was used to obtain higher resolution of the nanoparticle monolayers and measure the sizes and interparticle spacing (**Figures 1b&c**). An Asylum MFP3D atomic force microscope (AFM) equipped with AC240 cantilevers was used to obtain tapping mode images and force-indentation curves of the freestanding monolayers (**Figures 1d-f**). A cooler-heater accessory kit was installed on the AFM to change the sample temperature in an enclosed cell. For each temperature step, the sample was left for ~20mins to reach thermal equilibrium before AFM imaging and indentation. The AFM cantilever was calibrated at each temperature step to acquire accurate force-indentation data. AFM indentation and retraction curves were both recorded from the process, and the indentation data were analyzed to obtain the Young's modulus. The stiffness of bare carbon TEM grids without nanoparticle monolayers was also measured and subtracted from the force-indentation curves, thus only force responses from the freestanding monolayers were considered in the analysis.

Given the large size of the nanoparticle membrane system and the sequential nature of the runs required to understand their hysteretic behavior, an all atom model involving multi-million atom systems and over several tens of nanoseconds and multiple starting configurations would be computationally intractable. We therefore used a computational multiscale approach to generate an atomistic-informed coarse-grained model of dodecanethiol-ligated gold particles in the framework of the MARTINI force field. The MARTINI model provides a suitable level of coarse-graining, as it retains information about the chemistry specific to the alkanethiol ligands. In our framework, the gold nanoparticle core is represented by one bead (type Au), each dodecanethiol ligand by four beads (see below figure), and every four water molecules is represented by one bead. The non-bonded interactions between beads are modeled using Lennard-Jones potentials.

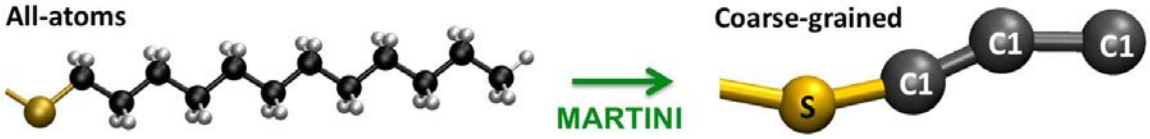

LJ	ε_{ij} (kcal/mol)	σ_{ij} (Å)	Bond/Angle	k (kcal/mol)	r_0/theta$_0$ (Å/deg)
C1, C1	0.836520	5.27557	C1 – C1	1.493786	4.7
C1, S	0.645315	5.27557	C1 – S	1.493786	4.7
S, S	1.075530	5.27557	Au – S	3.0	20.0
Au, C1	0.478011*	22.0	C1 – C1 – C1	2.987572	180.0
Au, S	1.195030*	22.0	C1 – C1 – S	2.987572	180.0
Au, Au	1.338430*	35.6			

* These values scaled by a factor of about 40 will give Young's modulus close to experimental value.

Atomistic structures of the dodecanethiol ligands were generated for partially ligated (ligand coverage 0.28 nm^2/ligand) and fully ligated (ligand coverage 0.22 nm^2/ligand) gold nanoparticles. The atomistic structures were coarse-grained and equilibrated in explicit solvent environment at a temperature of 300 K for 10 ns. MD simulations of a 4×4 gold nanoparticle array at an air-water interface were then performed using the MARTINI force field to obtain the self-assembled nanoparticle membrane configurations.

To simulate the force indentation experiments of nanoparticle membranes, we performed uniaxial tensile loading simulations using LAMMPS. The self-assembled nanoparticle membrane configurations were simulated without water (corresponds to dry nitrogen

environment in experiment) and underwent a heat-cool cycle (7°C – 87°C – 7°C) at a rate of ~0.4 °C/ns total of ~378 ns). At each temperature, the system was first equilibrated for 2 ns in an isothermal-isobaric ensemble (P = 1 bar) followed by a uniaxial tensile loading up to 2% strain at a strain rate of 2.5×10^{-4}/ns in a canonical ensemble. The Young's moduli at different temperatures were determined from the slope of the stress-strain curves.

Acknowledgements

The authors would like to acknowledge support from the NSF through grant DMR-1508110 and through the Chicago MRSEC under NSF DMR-1420709. Use of the Center for Nanoscale Materials, an Office of Science user facility, was supported by the U.S. Department of Energy, Office of Science, Office of Basic Energy Sciences, under Contract No. DE-AC02-06CH11357.

References

1. Mueggenburg, K. E.; Lin, X. M.; Goldsmith, R. H.; Jaeger, H. M. Elastic Membranes of Close-Packed Nanoparticle Arrays. *Nat. Mater.* **2007**, *6*, 656-660.
2. Cheng, W.; Campolongo, M. J.; Cha, J. J.; Tan, S. J.; Umbach, C. C.; Muller, D. A.; Luo, D. Free-Standing Nanoparticle Superlattice Sheets Controlled by DNA. *Nat. Mater.* **2009**, *8*, 519-525.
3. Cheng, W.; Campolongo, M. J.; Tan, S. J.; Luo, D. Freestanding Ultrathin Nano-Membranes via Self-Assembly. *Nano Today* **2009**, 6, 482-493.
4. Dong, A.; Chen, J.; Vora, P. M.; Kikkawa, J. M.; Murray, C. B. Binary Nanocrystal Superlattice Membranes Self-Assembled at The Liquid-Air Interface. *Nat. Mater.* **2010,** *466*, 474-477.
5. Talapin, D. V.; Lee, J. S.; Kovalenko, M. V.; Shevchenko, E. V. Prospects of Colloidal Nanocrystals for Electronic and Optoelectronic Applications. *Chem. Rev.* **2010**, *110*(1), 389.
6. Lee, J. S.; Kovalenko, M. V.; Huang, J.; Chung, D. S.; Talapin, D. V. Band-Like Transport, High Electron Mobility and High Photoconductivity in All-Inorganic Nanocrystal Arrays. *Nat. Nanotech.* **2011,** *6*, 348-352.

7. Kanjanaboos, P.; Lin, X. M.; Sader, J. E.; Rupich, S.; Jaeger, H. M.; Guest, J. R. Self-Assembled Nanoparticle Drumhead Resonators. *Nano Lett*. **2013**, *13*, 2158.
8. Rupich, S. M.; Castro, F. C.; Irvine, W. T. M.; Talapin, D. V. Soft Epitaxy of Nanocrystal Superlattices. *Nat. Comm*. **2014**, *5*, 5045.
9. Liao, J.; Blok, S.; van der Molen, S. J.; Diefenbach, S.; Holleitner, A. W.; Schönenberger, C.; Vladyka, A.; Calame, M. Ordered Nanoparticle Arrays Interconnected by Molecular Linkers: Electronic and Optoelectronic Properties. *Chem. Soc. Rev.* **2015,** *44*, 999.
10. Kovalenko, M. V.; Manna, L.; Cabot, A.; Hens, Z.; Talapin, D. V.; Kagan, C. R.; Klimov, V. I.; Rogach, A. L.; Reiss, P.; Milliron, D. J.; Sionnest, P. G.; Konstantatos, G.; Parak, W. J.; Hyeon, T.; Korgel, B. A.; Murray, C. B.; Heiss, W. Prospects of Nanoscience with Nanocrystals. ACS *Nano*. **2015**, *9*, 1012.
11. Schlicke, H.; Battista, D.; Kunze, S.; Schröter, C. J.; Eich, M.; Vossmeyer, T. Freestanding Membranes of Cross-Linked Gold Nanoparticles: Novel Functional Materials for Electrostatic Actuators. ACS *Appl. Mater. Interfaces* **2015**, *7*(28), 15123-15128.
12. Boles, M. A.; Engel, M.; Talapin, D. V. Self-Assembly of Colloidal Nanocrystals: From Intricate Structures to Functional Materials. *Chem. Rev.* **2016**, *116*(18), 11220-11289.
13. He, J.; Kanjanaboos, P.; Frazer, N. L.; Weis, A.; Lin, X. M.; Jaeger H. M. Fabrication and Mechanical Properties of Large-Scale Freestanding Nanoparticle Membranes. *Small* **2010**, *6*, 1449-1456.
14. Wang, Y.; Kanjanaboos, P.; Barry, E.; McBride, S. P.; Lin, X. M.; Jaeger, H. M. Fracture and Failure of Nanoparticle Monolayers and Multilayers. *Nano Lett*. **2014**, *14*, 826-830.
15. Wang, Y.; Kanjanaboos, P.; McBride, S. P.; Barry, E.; Lin, X. M.; Jaeger, H. M. Mechanical Properties of Self-Assembled Nanoparticle Membranes: Stretching and Bending. *Faraday Discuss.* **2015,** *181*, 328-338.
16. Luedtke, W. D.; Landman, U. Structure and Thermodynamics of Self-Assembled Monolayers on Gold Nanocrystallites. *J. Phys. Chem. B* **1998**, *102*, 6566-6572.

17. Landman, U.; Luedtke, W. D. Small is Different: Energetic, Structural, Thermal, and Mechanical Properties of Passivated Nanocluster Assemblies. *Faraday Discuss*. **2004**, 125, 1-22.
18. Schapotschnikow, P.; Pool, R.; Vlugt, T. J. H. Molecular Simulations of Interacting Nanocrystals. *Nano Lett*. **2008**, *8*, 2930-2934.
19. Salerno, K. M.; Bolintineanu, D. S.; Lane, J. M. D.; Grest, G. S. High Strength, Molecularly Thin Nanoparticle Membranes. *Phys. Rev. Lett*. **2014**, *113*, 258301.
20. Salerno, K. M.; Bolintineanu, D. S.; Lane, J. M. D.; Grest, G. S. Ligand Structure and Mechanical Properties of Single-Nanoparticle-Thick Membranes. *Phys. Rev.* E **2015**, *91*, 062403.
21. Salerno, K. M.; Grest, G. S. Temperature Effects on Nanostructure and Mechanical Properties of Single-Nanoparticle Thick Membranes. *Faraday Discuss*. **2015**, *181*, 339-354.
22. Jiang, Z.; He, J.; Deshmukh, S. A.; Kanjanaboos, P.; Kamath, G.; Wang, Y.; Sankaranarayanan, K. R. S.; Wang, J.; Jaeger, H. M.; Lin, X. M. Subnanometre Ligand-Shell Asymmetry Leads to Janus-Like Nanoparticle Membranes. *Nat. Mater*. **2015**, *14*, 912-917.
23. Lin, X. M.; Jaeger, H. M.; Sorensen, C. M.; Klabunde, K. J. Formation of Long-Range-Ordered Nanocrystal Superlattices on Silicon Nitride Substrates. *J. Phys. Chem*. **2001**, *105*(17), 3353-3357.
24. Kanjanaboos, P.; Joshi-Imre, A.; Lin, X. M.; Jaeger, H. M. Strain Patterning and Direct Measurement of Poisson's Ratio in Nanoparticle Monolayer Sheets. Nano Lett. **2011**, *11*, 2567-2571.
25. Zhou, C.; Trionfi, A.; Hsu, J. W. P.; Walker, A. V. Electron-Beam-Induced Damage of Alkanethiolate Self-Assembled Monolayers (SAMs): Dependence on Monolayer Structure and Substrate Conductivity. *J. Phys. Chem.* C, **2010**, *114*, 9362-9369.
26. Bonthuis, D. J.; Gekle, S.; Netz, R. R. Dielectric Profile of Interfacial Water and its Effect on Double-Layer Capacitance. *Phys. Rev. Lett*. **2011**, *107*, 166102.
27. Zhang, C.; Gygi, F.; Galli G. Strongly Anisotropic Dielectric Relaxation of Water at the Nanoscale. *J. Phys. Chem. Lett.* **2013**, *4*, 2477-2481.